CrystEngComm

Accepted Manuscript

ROYAL SOCIETY OF CHEMISTRY

www.rsc.org/crystengcomm

Electrospun hollow cage-like α-Fe_2O_3 microspheres: synthesis, formation mechanism, and the morphology-reserved conversion to Fe nanostructures

Liqun Wang[a], *Xuegang Lu*[a]*, *Chang Han*[a], *Ruie Lu*[a], *Sen Yang*[a], *and Xiaoping Song*[a]*

School of Science, Key Laboratory of Shaanxi for Advanced Materials and Mesoscopic Physics, State Key Laboratory for Mechanical Behavior of Materials, Xi'an Jiaotong University, Xi'an 710049, ShaanXi, People's Republic of China.

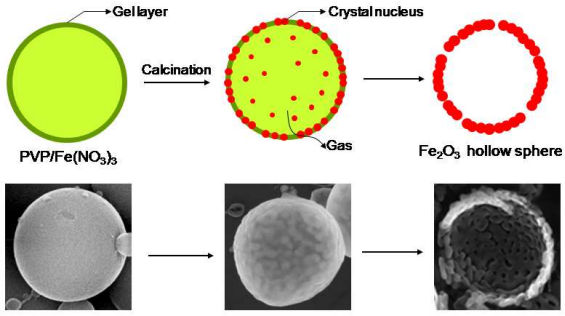

Novel 3D cage-like hollow α-Fe_2O_3 and Fe microspheres are fabricated by electrospinning followed by annealing process for the first time.

Cite this: DOI: 10.1039/coxx00000x

www.rsc.org/xxxxxx

PAPER

Electrospun hollow cage-like α-Fe_2O_3 microspheres: synthesis, formation mechanism, and the morphology-reserved conversion to Fe nanostructures

Liqun Wang[a], Xuegang Lu[a]*, Chang Han[a], Ruie Lu[a], Sen Yang[a], and Xiaoping Song[a]*

Received (in XXX, XXX) Xth XXXXXXXXX 20XX, Accepted Xth XXXXXXXXX 20XX
DOI: 10.1039/b000000x

Hollow cage-like α-Fe_2O_3 microspheres with average diameter of 500 nm and shell thickness of 60 nm are successfully synthesized by a simple electrospinning technique using ferric nitrate ($Fe(NO)_3 \cdot 9H_2O$) and polyvinyl pyrrolidone (PVP) precursor. $Fe(NO)_3$/PVP composite microspheres are calcined at high temperature to form an interconnected 3D cage-like hollow α-Fe_2O_3 structure. X-ray diffraction (XRD), field emission scanning electron microscopy (FE-SEM), high-resolution transmission electron microscopy (HR-TEM), and magnetic measurements are used to characterize the morphology, structure, and magnetic properties of α-Fe_2O_3 microspheres. Based on the characterization results, a formation mechanism for electrospun cage-like α-Fe_2O_3 hollow microspheres is proposed. We also find that morphology-preserved conversion from α-Fe_2O_3 to magnetic Fe can be achieved during the reduction reactions in H_2/Ar. The magnetic property investigation shows that the as-prepared Fe hollow nanostructures exhibit a ferromagnetic behavior and possess a high saturation magnetization (M_s).

Introduction

Nanostructured magnetic materials with desired size and shape play an important role in modern science and technology. Amongst various nanostructured materials, highly crystalline magnetic hollow nanostructures with various sizes and morphologies are attracting considerable attention due to their low effective density, high specific surface area, better permeation, intriguing size and shape-dependent properties, and attractive potential applications in the fields of magnetics,[1-3] catalysis,[4-6] water treatment,[7-9] energy storage,[10-13] drug-delivery,[14] synthesis of other nanocomposites,[15-17] and so on. For instance, the large fraction of void space in magnetic hollow structures can be used to load and control releasing systems for special materials, such as drugs, genes, and biological molecules. They can also be used to modulate refractive index for photonic crystal, lower density for electromagnetic absorber, increase active area for catalysis, improve the particles' ability for the removal of toxic heavy metal ions and organic pollutants from wastewater. So far, numerous methods have been developed to synthesize hollow structures of many materials, including template-assisted synthesis,[18] direct evacuation with Ostwald ripening,[19, 20] and the Kirkendall effect.[21] For example, template methods are extensively employed to prepare hollow structures. However, both of the hard and soft template-assisted synthesis methods usually require high-cost and tedious procedures, including template modification, precursor attachment, and core removal. So, it is still a great challenge to develop low-cost, environmentally friendly, simple, and versatile approaches for synthesis of hollow micro- and nanostructures that will greatly facilitate the future application of these hollow structures in various fields.

Iron oxide materials have great natural abundance and excellent environmental compatibility. In particular, hematite (α-Fe_2O_3), an n-type semiconductor with 2.1 eV band gap, has attracted much attention due to its low-cost, non-toxicity, high resistance to corrosion, environmentally friendly characters, and widespread application as catalyst, pigment, sensor, and the raw material for the synthesis of γ-Fe_2O_3 and Fe.[4, 22-24] In addition to conventional applications, hollow α-Fe_2O_3 structures may also be used for encapsulation of various guest molecules, and this is likely to lead to novel applications in areas such as functional materials and medicine carrier. Although hematite hollow structures with various shapes, such as spheres,[25-27] peanuts,[28] rings,[29, 30] tubes,[31] and spindles,[32] have already been synthesized, the methods to obtain these hollow structures usually need a complex and a multistep process to obtain the final product. In some cases, the yield of hollow structures is low. In recent years, electrospinning has been extensively explored as an advantageous and easy method to create various metal oxide hollow fibers with diameters ranging from tens of nanometres to several micrometres.[33-37] However, to the best of our knowledge, there are no reports about hollow cage-like α-Fe_2O_3 microspheres prepared by electrospinning. Even though the formation process of beads was observed but their presence had been considered to be an avoidable fiber imperfection.[38] In particular, up to the present no works about hollow cage-like Fe microspheres have been reported. Hollow cage-like α-Fe_2O_3 microspheres, especially hollow cage-like Fe microspheres have great potential to be used in many crucial areas, such as catalysis, water treatment, energy storage, drug-delivery, microwave absorber etc. So, the synthesis of hollow cage-like α-Fe_2O_3 and Fe microspheres is of great interest.

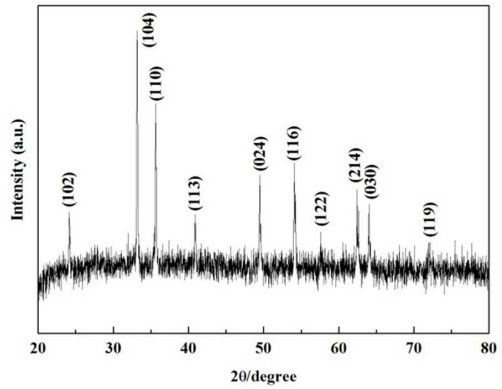

Fig. 1 XRD pattern of the obtained α-Fe_2O_3 sample.

In this paper, we first present the fabrication of cage-like α-Fe_2O_3 hollow microspheres by directly annealing electrospun PVP/$Fe(NO_3)_3$ composite microspheres. Compared with other methods, neither a coating procedure nor a special spinner is required, hollow microspheres can be synthesized by simply annealing composite microspheres at high temperature with an appropriate heating rate. Furthermore, as-prepared α-Fe_2O_3 hollow microspheres can be converted to Fe by a subsequent reduction process while preserving the cage-like morphology. The morphology, microstructure and magnetic properties of the cage-like α-Fe_2O_3 and Fe hollow microspheres are investigated in detail.

Experimental

Preparation of sample

All the chemicals used were analytical grade and without further purification. In a typical procedure, 1.8 g of polyvinyl pyrrolidone (PVP) was added to 2 ml of ethanol and 5 ml of N, N–dimethylformamide and the mixture was magnetically stirred for 3 h to form a clear solution. Then, a certain amount of 0.2 M ferric nitrate ($Fe(NO)_3 \cdot 9H_2O$) solution was added dropwise into the above solution under continuous magnetic stirring. After stirring for 5h, the mixed solution was then transferred into a plastic syringe with a spinneret of 0.8 mm. A tip-to-collector distance of 15 cm and a voltage of 18 kV were applied during electrospinning. The as-electrospun $Fe(NO)_3$/PVP composite microspheres were calcined at 450~950 ℃for 2 h in the muffle furnace with a heating rate of 5℃/min to form 3D cage-like hollow structures. The effect of reaction duration on the morphology of α-Fe_2O_3 was discussed. The cage-like Fe nanostructures were prepared via a reduction process with the corresponding α-Fe_2O_3 products as starting materials. The dried α-Fe_2O_3 powders were annealed in a furnace at 380 ℃ under a continuous hydrogen/argon gas flow [$H_2/(H_2+Ar)$=8/100] for 5 h. Then the furnace was allowed to cool to room temperature while still under a continuous hydrogen gas flow.

Characterization

The crystal structure of the obtained products was determined by powder X-ray diffraction (XRD) analysis using Cu K_α radiation. Morphology was analyzed using a high-resolution transmission electron microscopy (HRTEM) on a JEOL-2100 transmission electron microscope operating at 200 kV and a field emission scanning electron microscopy (FE-SEM, JSM-7000F). Magnetization data was taken through a Quantum Design SQUID magnetometer. The temperature dependence of magnetization (M-T) was measured under zero-field-cooling (ZFC) and field-cooling (FC) conditions from 2 K to 300 K by applying a magnetic field of 100 Oe. The field dependence of magnetization (M-H) was examined at 2 and 300 K with a continuous field sweeping from -30 to 30 kOe.

Results and discussion

The XRD pattern of the α-Fe_2O_3 sample calcined at 800 ℃ for 2 h is shown in Fig. 1. It can be seen that all of the diffraction peaks can be indexed to a pure rhombohedral phase of α-Fe_2O_3 (hematite) [space group: *R*-3c (JCPDS, No. 33-0664)] with cell constants of a=0.5035 nm and c=1.3740 nm. Hematite possesses a rhombohedrally centered hexagonal structure with close packed oxygen lattice. The sharp diffraction peaks indicate that the as-obtained sample is well crystallized. No other diffraction peaks are observed for impurities such as β-FeOOH, Fe_3O_4, or γ-Fe_2O_3.

The morphology and structure of as-prepared product obtained at 800℃ were investigated by using FE-SEM and TEM as shown in Fig. 2. Fig. 2a shows the representative low-magnification SEM image of the product, which indicates that spherical α-Fe_2O_3 particles with diameter of 100-800 nm are obtained on a large scale. On further inspection by the means of high-magnification SEM image (Fig. 2b and insert), it is found that as-prepared α-Fe_2O_3 particles possess cage-like structure with a hollow interior. The cage-like surfaces are made up of interconnected nanoparticles from 40-80 nm in size. The thickness of the shell is about 60 nm. More morphology and structure details of the cage-like hollow microspheres are further elucidated by TEM result, as shown in Fig. 2c. From the brightness contrast of interior and outer shell, the hollow morphology with an average diameter of about 500 nm can be observed, which confirms the FESEM results. The HRTEM image of the cage-like surface (Fig. 2d) shows clear crystalline fringes with an interplanar distance of 0.251 and 0.221 nm, consistent with the spacing distance between α-Fe_2O_3 $(1\bar{2}0)$ and (113) lattice planes, which confirms the shell components of α-Fe_2O_3 nanocrystals and also demonstrates good crystallinity of α-Fe_2O_3 composition. The insert in Fig. 2d shows the corresponding sharp SAED patterns on individual α-Fe_2O_3 particle (insert in Fig. 2d), which indicates that the product is single crystalline in nature. The hollow sphere is composed of Orented aggregated nanocrystal particles with sizes of about 40-50 nm.

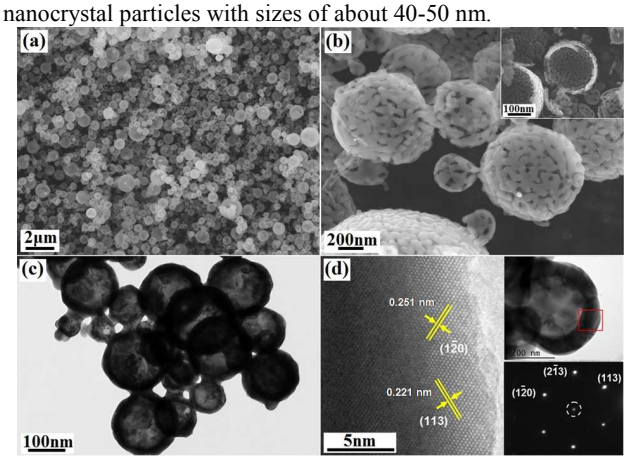

Fig. 2 (a) Low-magnification SEM image, (b) High-magnification SEM image and (insert) broken microspheres, (c) TEM image, (d) HRTEM image and (insert) TEM and SAED pattern of the α-Fe_2O_3 microspheres calcined at 800 ℃ for 2 h.

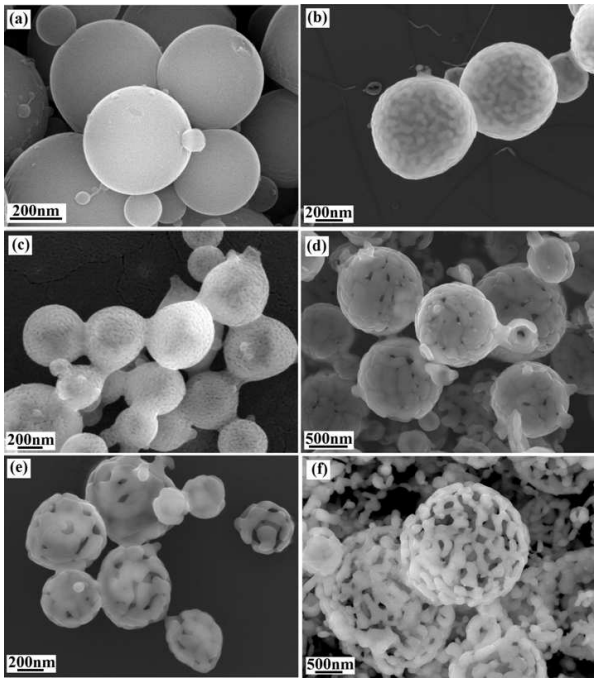

Fig. 3 SEM images of (a) precursor spheres before calcination, (b-f) α-Fe_2O_3 spheres calcined at 450℃, 500 ℃, 600℃, 800 ℃ and 950℃, respectively.

The effects of experiment parameters on the morphology of α-Fe_2O_3 product were attempted systematically, and the results revealed that the calcination temperature played a key role in the formation of cage-like hollow structure. In order to investigate the evolution process of the cage-like α-Fe_2O_3 spheres in more detail, experiments were carried out at different calcination temperatures from 450 ℃ to 900 ℃ for 2 h. Fig. 3 presents the typical SEM images of the microspheres for different calcination temperatures and the evolving process can be observed distinctly. Originally, precursor spheres with smooth surface formed after electrospinning, as shown in Fig. 3a. When the precursor is annealed at 450℃, the surface of spheres becomes coarse. When the temperature is further increased to 500℃, small pitting appears and instead of the pitting, obvious holes present at 600℃, as shown in Fig. 3c,d. Continuously, the pores distributed around the spheres surface become larger and cage-like hollow structure is obtained with increasing the temperature to 800℃, which can be seen in Fig. 3e and Fig. 2b. Fig. 3f exhibits the morphology of the cage-like hollow spheres which are obtained at 950℃. It can be seen that the cage-like structure is perfect but broken for some part. Obviously, the cage-like structure would presumably be broken into small particles when the temperature is even higher.

Based on the above experimental results, a reasonable formation mechanism is proposed. As we all known, electrospinning is a simple and versatile method to synthesize tubular structure of metal oxide.[33, 35, 39-41] However, during electrospun, the polymer solution flowing through the capillary is distorted into a Taylor cone under the electric field. When the viscoelasticity of the polymer solution is suitable, the shape of the initial smooth jet changes to a dumbbell-like jet, which can be described as two large drops connected by a thinner jet between them.[38] If the thinner jet is not resistant enough, it breaks and beads are formed.[42] As a result, instead of fibers, PVP/$Fe(NO_3)_3$ precursor microspheres are obtained on the collector, as shown in Fig. 3a and Figure S1.

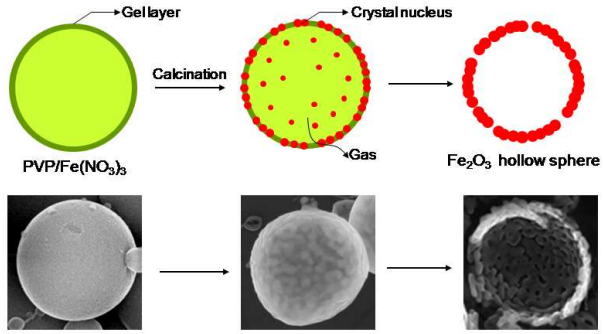

Scheme 1. The formation process of hollow-cage α-Fe_2O_3 microsphere.

In the electrospinning process, the evaporation of solvents would result in the formation of a gel layer on the surface of the PVP/$Fe(NO_3)_3$ precursor microspheres. This gel layer has an important function to maintain the sphere structure during heat treatment. With following calcination, the Fe^{3+} located on or near the surface of the precursor microspheres begin to react with O_2 to form α-Fe_2O_3 nucleus, while most of the Fe^{3+} in the core region is relatively difficult to react due to lack of oxygen. Therefore, an obvious Fe^{3+} concentration gradient forms in the section of electrospun microspheres, which will drive Fe^{3+} to diffuse to the surface and transform to α-Fe_2O_3 nanoparticles. In the meantime, another concentration gradient of α-Fe_2O_3 nucleus also exists from the surface to the core. If the calcination is proceeding, owing to the crystal growth via Oswald-ripening and Fe^{3+} ion diffusion, the crystal nucleus and nitrate precursors will migrate from the inner core to the outer layer. In addition, PVP is also important to the formation of hollow α-Fe_2O_3 microspheres. During calcination, a large number of gas (e.g. CO_x) will be generated through decomposing of PVP. The diffusion of the gas from the inner core to the outer surface will push the inner crystal nucleus and nitrate precursors to the outer layer of the microspheres, which leads to form hollow structure. On the basis of above discussion, we can conclude that the crystal growth via Oswald-ripening and the diffusion of Fe^{3+} ion driven by concentration gradient as well as the "gas push" effect are the crucial parameters for the formation of hollow cage-like α-Fe_2O_3 microspheres. The transition process is exhibited in scheme 1. Moreover, it is believed that with the movement of α-Fe_2O_3 nuclues to the surface of spheres, they connect with each other through the Oriented-attachment process,[43] so that single crystalline α-Fe_2O_3 shells are formed.

Magnetic materials with cage-like hollow structure have great potential to be used in some important areas such as drug delivery, water treatment, and microwave absorbtion etc. However, the weak ferromagnetic properties of α-Fe_2O_3 limit their performance in these areas. To improve the magnetic property of products, the dried cage-like α-Fe_2O_3 microspheres were annealed in a furnace under a continuous H_2/Ar mixed gas flow. After reaction at 380℃ for 3h, the α-Fe_2O_3 was converted to Fe. The morphology and phase structure of as-obtained Fe powders were analyzed by SEM, TEM, and XRD technique, as shown in Fig. 4. It is evident from SEM images (Fig. 4a and b) that the morphology of the α-Fe_2O_3 microspheres can be perfectly preserved during the conversion from α-Fe_2O_3 to Fe. The conversion is highly efficient, and a large quantity of cage-like Fe microspheres can be produced. From TEM image (Fig. 4c), it can be observed that as-prepared

Fe microspheres have clear hollow interior voids, indicating that the hollow structure is successfully maintained. Interestingly, the ring-like SAED patterns (insert in Fig. 4c) reveal that the Fe microspheres possess polycrystalline structure, rather than single-crystal structure of previous α-Fe_2O_3. The XRD patterns of the Fe microspheres (Fig. 4d) confirm the high crystallinity of the products, all of which are well-indexed to the pure body-centered structure of Fe (JPCDS no. 06-0696).

To evaluate the conversion degree from α-Fe_2O_3 to magnetic Fe hollow microspheres, Raman spectra of as-prepared hollow microspheres before and after H_2 reduction were measured respectively, as shown in Fig. 5. It can be seen that for the α-Fe_2O_3 sample before H_2 reduction, five strong resonant peaks at about 221, 287, 401, 493, and 601 cm^{-1} in the range of 200-800 cm^{-1} all correspond to peaks for α-Fe_2O_3.[44] However, after H_2 reduction, no evident resonant peaks corresponding to polymorphs of Fe(III) oxide or oxyhydroxide (e.g., α-Fe_2O_3,γ-Fe_2O_3, α-FeOOH, γ-FeOOH), can be detected. In addition, neither spectra show a peak at 660 cm^{-1} that can indicate the presence of Fe_3O_4.[24, 45, 46] This indicates that the conversion degree from α-Fe_2O_3 to magnetic Fe hollow microspheres is very high so that nearly all α-Fe_2O_3 phases have been conversed to Fe. No Fe_3O_4, α-Fe_2O_3 or γ-Fe_2O_3 appeared or remained in the final Fe products.

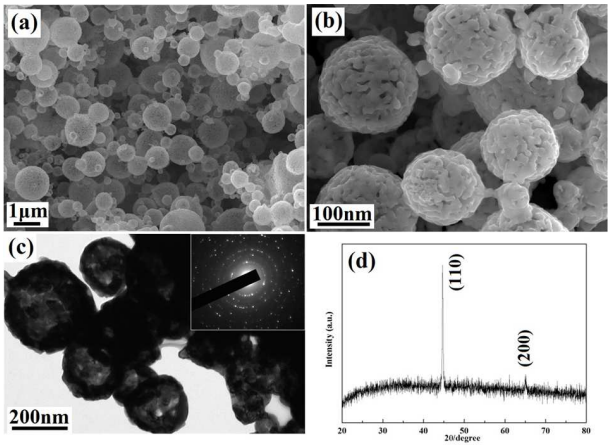

Fig. 4 (a) SEM image, (b) High-magnification SEM image, (c) TEM image and SAED patterns (inset), and (d) XRD patterns of Fe microspheres. The morphology of the initial microspheres was maintained during the conversion from α-Fe_2O_3 to Fe.

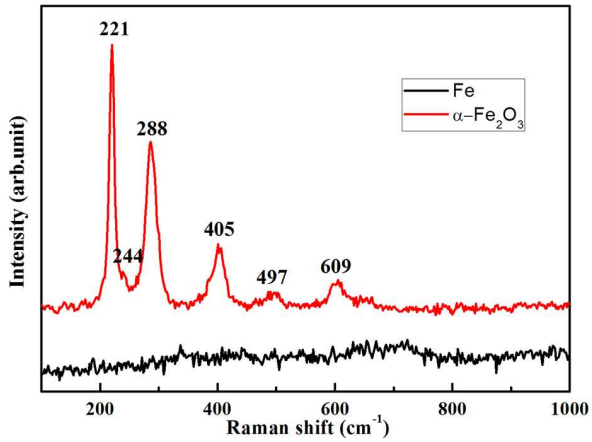

Fig. 5 The Raman spectra of the as-prepared a-Fe_2O_3 and Fe microspheres. The laser wave length was 514 nm.

The magnetic properties of the synthesized α-Fe_2O_3 and Fe samples were examined by a Quantum Design superconducting quantum interference device (SQUID). The temperature dependence of magnetization (M-T) was measured with zero-field cooling (ZFC) and field cooling (FC) methods in an applied magnetic field of 100 Oe between 2 K and 400 K. For zero field cooled magnetization measurements, the sample was first cooled to 2 K. After applying a 100 Oe field at 2 K, the magnetization was measured in the warming cycle. For field-cooled magnetization measurements, the sample was cooled in the same field (100 Oe) to 2 K, and the magnetization was measured in the warming cycle under the field. The rate of cooling was constant in both ZFC and FC conditions.

Fig. 6a shows the M-T curve of the cage-like α-Fe_2O_3 microspheres. A splitting between the FC and ZFC curves suggests the presence of the long-range magnetic order in the cage-like α-Fe_2O_3 microspheres and the blocking temperature exceeds the temperature of 380 K. It has been known that the bulk hematite is antiferromagnetic (AFM) below a first-order magnetic transition temperature T_M (the Morin transition temperature, about 260K) and in a weak ferromagnetic (FM) state between T_M and T_N (Néel temperature, about 950 K). The T_M can be influenced by numerous factors, such as crystal defects, strains, surface phenomena, and particle size. Normally, the unideal crystallinity would usually suppress the reorientation transition of the moments at the two sublattice sites, changing from a canted alignment within the a-b basal plane (weak FM state) to an antiparallel alignment along the c-axis (AFM state). With our as-prepared α-Fe_2O_3 microspheres, however, T_M occurs at about 260 K, as revealed by the sharp feature in the FC and ZFC curves (Fig. 6a), indicating a well crystallized condition for the cage-like microspheres, as already shown by the HRTEM images in Fig. 2d.

Fig. 6b shows the hysteresis loops of the α-Fe_2O_3 microspheres at 2 K and 300 K. It can be seen that both magnetization curves show ferromagnetic behavior. The remnant magnetization and coercivity of the cage-like α-Fe_2O_3 microspheres at 2 K are 1.7 emu g^{-1} and 314 Oe, respectively, and at 300 K the values are 0.3 emu g^{-1} and 50 Oe, respectively. The magnetic hysteresis curves measured at different temperatures are saturated within the applied field, and the saturation magnetization (M_s) at 2 and 300 K are 6.0 and 3.9 emu g^{-1}, respectively. The coercivity and remnant magnetization at 2 K is greater than at 300 K, indicating that the magnetocrystalline anisotropy constant increases with the decreasing temperature and the magnetic moment may get further freezing and the magnetic region may change.[47, 48]

After morphology-preserved conversion from α-Fe_2O_3 to magnetic Fe, the magnetic behavior changed significantly. Fig. 6c shows the M-T curve of the cage-like Fe microspheres. It can be seen the ZFC magnetisation increases rapidly upon heating for low temperatures below 50 K. At higher temperatures, there is a region of linear increase. The ZFC and FC curves separate from each other with the temperature going up to 380 K, indicating the presence of an anisotropy barrier and ferromagnetism is present up to at least 380 K. For higher temperatures, due to the thermal activation effect against the barrier, we expect superparamagnetic behaviour. The sharp increase of the ZFC magnetization at very low temperatures below 50 K is speculated to be due to the defreezing of the frozen moment in the surface layer of small Fe particles.[49]

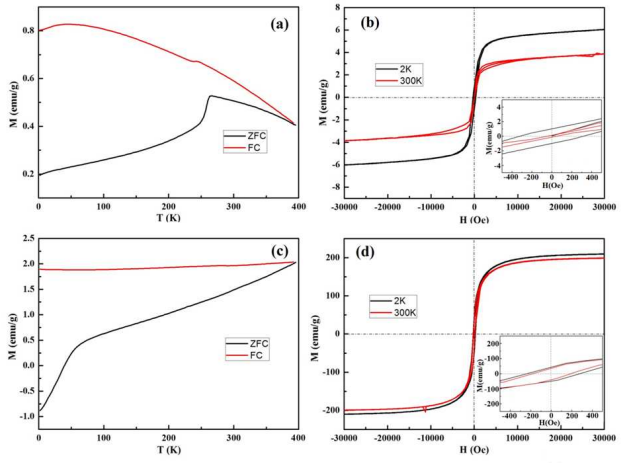

Fig. 6 (a) ZFC and FC (at 100Oe) curves of α-Fe_2O_3; (b) M-H curves at 2 K and 300K of α-Fe_2O_3; (c) ZFC and FC (at 100 Oe) curves of Fe; (d) M-H curves at 2 K and 300 K of Fe.

The hysteresis loops of the Fe microspheres measured at 2 K and 300 K (Fig. 6d) show typical ferromagnetic behaviours with non-zero remnant magnetization and coercivity. The magnetic saturation is reached with the external field exceeding 30 kOe. It shows a value of saturation magnetization of about 213.6 emu g^{-1} and coercivity about 260 Oe for the loop at 2 K, whereas for the loop at 300 K, the values are 201.9 emu g^{-1} for the saturation magnetization and 180 Oe for the coercivity. The saturation magnetization measured at 2 K for cage-like Fe microspheres is close to the bulk iron magnetization. The little difference of M_s at 2 K and 300 K is inclined to the results of M–T measurement also. Because the T_c of the samples is much higher than 300 K, the Fe samples at 2 K and 300 K have spontaneous magnetism due to the molecular field (H_{mol}), and $\mu_0\mu_B H_{mol}/K_BT >> 1$ (here μ_0 and μ_B referred to magnetic constant and Bohr magneton, respectively), which means that the thermal perturbation shows little effect on the M_s compared with external field H_{ext}, and so the measured M_s of the samples are similar to each other at 2 and 300 K.[50]

Conclusions

In summary, this paper presents an a simple electrospinning technique that demonstrates for the first time the fabrication of high yield crystalline cage-like α-Fe_2O_3 hollow microspheres. After calcination at high temperature, $Fe(NO)_3$/PVP composite microspheres are converted to interconnected 3D cage-like hollow α-Fe_2O_3 structure. It is also found that morphology-preserved conversion from α-Fe_2O_3 to magnetic Fe can be achieved during the reduction reactions in H_2/Ar. The magnetic property investigation shows that the as-prepared Fe hollow nanostructures exhibit a ferromagnetic behavior and possess a high saturation magnetization (*Ms*).

Acknowledgements

We are grateful for financial support from the National Natural Science Foundation of P. R. China (No. 51172178, 51222104, 51371134)

Notes and references

[a] *School of Science, Key Laboratory of Shaanxi for Advanced Materials and Mesoscopic Physics, State Key Laboratory for Mechanical Behavior of Materials, Xi'an Jiaotong University, Xi'an 710049, ShaanXi, People's Republic of China. Fax: 01-86-29-82663034; Tel: 01-86-29-82663034; E-mail: xglu@mail.xjtu.edu.cn (Xuegang Lu), xpsong@mail.xjtu.edu.cn (Xiaoping Song)*

1. N. Wang, X. Cao, D. Kong, W. Chen, L. Guo and C. Chen, *J. Phys. Chem. C*, 2008, **112**, 6613-6619.
2. D. Du and M. Cao, *J. Phys. Chem. C*, 2008, **112**, 10754-10758.
3. Z. H. Yang, Z. W. Li, J. Zhao and Y. H. Yang, *Rsc Advances*, 2014, **4**, 9457-9462.
4. X. Li, X. Yu, J. He and Z. Xu, *J. Phys. Chem. C*, 2009, **113**, 2837-2845.
5. S. Xuan, W. Jiang, X. Gong, Y. Hu and Z. Chen, *J. Phys. Chem. C*, 2009, **113**, 553-558.
6. C. Song, W. Yu, B. Zhao, H. Zhang, C. Tang, K. Sun, X. Wu, L. Dong and Y. Chen, *Catal. Commun*, 2009, **10**, 650-654.
7. Y. Liu, Y. Wang, S. Zhou, S. Lou, L. Yuan, T. Gao, X. Wu, X. Shi and K. Wang, *Acs Appl. Mater. Inter.*, 2012, **4**, 4913-4920.
8. Z. Wei, R. Xing, X. Zhang, S. Liu, H. Yu and P. Li, *Acs Appl. Mater. . Inter.*, 2013, **5**, 598-604.
9. B. Zou, Y. Liu and Y. Wang, *Rsc Advances*, 2013, **3**, 23327-23334.
10. J. Zhang, Y. Yao, T. Huang and A. Yu, *Electrochim. Acta*, 2012, **78**, 502-507.
11. H. Jun-Ki, L. Hyung-Seok, S. Yang-Kook and S. Kyung-Do, *J.Power Sources*, 2013, **244**, 538-543.
12. Z. Qiumei, S. Zhicong, D. Yuanfu, Z. Jun, L. Guichang and C. Guohua, *J.Power Sources*, 2012, **197**, 305-309.
13. R. Liu, S. Yang, F. Wang, X. Lu, Z. Yang and B. Ding, *Acs Appl. Mater.Inter.*, 2012, **4**, 1537-1542.
14. D. Li, J. Tang, J. Guo, S. Wang, D. Chaudhary and C. Wang, *Chem. Eur. J.*, 2012, **18**, 16517-16524.
15. L. Chun-Rong, I. H. Chen, W. Cheng-Chien and C. Mei-Li, *Acta Mater.*, 2011, **59**, 6710-6716.
16. X. Luo, S. Lian, L. Wang, S. Yang, Z. Yang, B. Ding and X. Song, *Crystengcomm*, 2013, **15**, 2588-2591.
17. J. Chen, W. Yan, C. X. Liu, R. G. Ding and X. H. Fan, *Mater. Charact.*, 2011, **62**, 237-242.
18. F. Caruso, R. A. Caruso and H. Mohwald, *Science*, 1998, **282**, 1111-1114.
19. Z. Hua Chun, *J. Mater. Chem.*, 2006, **16**, 649-662.
20. X. Yang, J. Fu, C. Jin, J. Chen, C. Liang, M. Wu and W. Zhou, *J. Am. Chem. Soc.*, 2010, **132**, 14279-14287.
21. A.-Q. Zhang, H.-J. Li, D.-J. Qian and M. Chen, *Nanotechnology*, 2014, **25**.
22. J. Chen, L. N. Xu, W. Y. Li and X. L. Gou, *Adv. Mater.*, 2005, **17**, 582.
23. N. Pailhe, A. Wattiaux, M. Gaudon and A. Demourgues, *J. Solid State Chem.*, 2008, **181**, 2697-2704.
24. X. Zhang, Y. Niu, X. Meng, Y. Li and J. Zhao, *Crystengcomm*, 2013, **15**, 8166-8172.
25. P. Sun, Z. Zhu, P. Zhao, X. Liang, Y. Sun, F. Liu and G. Lu, *Crystengcomm*, 2012, **14**, 8335-8337.

26. J. Zhu, Z. Yin, D. Yang, T. Sun, H. Yu, H. E. Hoster, H. H. Hng, H. Zhang and Q. Yan, *Energy. Environ. Sci.*, 2013, **6**, 987-993.
27. S. Xu, C. M. Hessel, H. Ren, R. Yu, Q. Jin, M. Yang, H. Zhao and D. Wang, *Energy. Environ. Sci.*, 2014, **7**, 632-637.
28. Z. An, J. Zhang, S. Pan and G. Song, *Powder Technol.*, 2012, **217**, 274-280.
29. L. Li, Y. Chu and Y. Liu, *Nanotechnology*, 2007, **18**.
30. C.-J. Jia, L.-D. Sun, F. Luo, X.-D. Han, L. J. Heyderman, Z.-G. Yan, C.-H. Yan, K. Zheng, Z. Zhang, M. Takano, N. Hayashi, M. Eltschka, M. Klaeui, U. Ruediger, T. Kasama, L. Cervera-Gontard, R. E. Dunin-Borkowski, G. Tzvetkov and J. Raabe, *J. Am. Chem. Soc.*, 2008, **130**, 16968-16977.
31. L. Lu, K. Hui-Zhong, M. Wenling, L. Huajie and W. Yuqiu, *J. Phys. Chem. B*, 2006, **110**, 15218-15223.
32. C. Frandsen, B. A. Legg, L. R. Comolli, H. Zhang, B. Gilbert, E. Johnson and J. F. Banfield, *Crystengcomm*, 2014, **16**, 1451-1458.
33. L. Lang and Z. Xu, *Chem. Lett.*, 2013, **42**, 750-752.
34. G. Binitha, M. S. Soumya, A. A. Madhavan, P. Praveen, A. Balakrishnan, K. R. V. Subramanian, M. V. Reddy, S. V. Nair, A. S. Nair and N. Sivakumar, *J. Mater. Chem. A*, 2013, **1**, 11698-11704.
35. Y. Cheng, B. Zou, C. Wang, Y. Liu, X. Fan, L. Zhu, Y. Wang, H. Ma and X. Cao, *Crystengcomm*, 2011, **13**, 2863-2870.
36. J.-M. Li, X.-L. Zeng, Y.-H. Dong and Z.-A. Xu, *Crystengcomm*, 2013, **15**, 2372-2377.
37. J. Guan, F. Mou, Z. Sun and W. Shi, *Chem. Commun..*, 2010, **46**, 6605-6607.
38. W. W. Zuo, M. F. Zhu, W. Yang, H. Yu, Y. M. Chen and Y. Zhang, *Polym. Eng. Sci.*, 2005, **45**, 704-709.
39. X. Chen, K. M. Unruh, C. Ni, B. Ali, Z. Sun, Q. Lu, J. Deitzel and J. Q. Xiao, *J. Phys. Chem. C*, 2011, **115**, 373-378.
40. J.-M. Li, X.-L. Zeng, A.-D. Mo and Z.-A. Xu, *Crystengcomm*, 2011, **13**, 6964-6967.
41. J.-M. Li, X.-L. Zeng and Z.-A. Xu, *Appl. Phys. Lett.*, 2013, **103**.
42. D. Fantini, M. Zanetti and L. Costa, *Macromol. Rapid Commun.*, 2006, **27**, 2038-2042.
43. Y. Zhu, W. Zhao, H. Chen and J. Shi, *J. Phys. Chem. C*, 2007, **111**, 5281-5285.
44. S. Z. Li, H. Zhang, J. B. Wu, X. Y. Ma and D. R. Yang, *Cryst. Growth Des.*, 2006, **6**, 351-353.
45. R. L. Spray and K.-S. Choi, *Chem. Mater.*, 2009, **21**, 3701-3709.
46. J. M. Li, A. C. H. Huan, L. Wang, Y. W. Du and D. Feng, *Phys. Rev. B*, 2000, **61**, 6876-6878.
47. Y. Y. Xu, X. F. Rui, Y. Y. Fu and H. Zhang, *Chem. Phys. Lett.*, 2005, **410**, 36-38.
48. R. Amutha, M. Muruganandham, M. Sathish, S. Akilandeswari, R. P. S. Suri, E. Repo and M. Sillanpaa, *J. Phys. Chem. C*, 2011, **115**, 6367-6374.
49. W. Ning, C. Xia, K. Desheng, C. Weimeng, G. Lin and C. Chinping, *J. Phys. Chem. C*, 2008, **112**, 6613-6619.
50. M. Respaud, J. M. Broto, H. Rakoto, A. R. Fert, L. Thomas, B. Barbara, M. Verelst, E. Snoeck, P. Lecante, A. Mosset, J. Osuna, T. Ould-Ely, C. Amiens and B. Chaudret, *Phys. Rev. B*, 1998, **57**, 2925-2935.

